The Role of Ligand Density and Size in Mediating Quantum Dot Nuclear Transport

*Peter S. Tang, Sarmitha Sathiamoorthy, Lindsay C. Lustig, Romina Ponzielli, Ichiro Inamoto, Linda Z. Penn, Jumi A. Shin, and Warren C. W. Chan**

***S**tudying the effects of the physicochemical properties of nanomaterials on cellular uptake, toxicity, and exocytosis can provide the foundation for designing safer and more effective nanoparticles for clinical applications. However, an understanding of the effects of these properties on subcellular transport, accumulation, and distribution remains limited. The present study investigates the effects of surface density and particle size of semiconductor quantum dots on cellular uptake as well as nuclear transport kinetics, retention, and accumulation. The current work illustrates that cellular uptake and nuclear accumulation of nanoparticles depend on surface density of the nuclear localization signal (NLS) peptides with nuclear transport reaching a plateau at 20% surface NLS density in as little as 30 min. These intracellular nanoparticles have no effects on cell viability up to 72 h post treatment. These findings will set a foundation for engineering more sophisticated nanoparticle systems for imaging and manipulating genetic targets in the nucleus.*

1. Introduction

The nano–bio interaction has received significant attention in recent years as research groups aim to correlate the physicochemical parameters of nanoparticles with biological responses.[1] Such correlation will enable rational design of nanoparticles with desired functionalities. These parameters include ligand density,[2] size,[3–5] and surface charge,[6–8] which have been demonstrated to affect cellular uptake of nanoparticles. Most studies to date have focused on elucidating the biodistribution and cellular interactions of nanoparticles of different physicochemical properties. There have been limited studies on the role of nanoparticle design in mediating subcellular transport. Studies along this line will provide a basis to optimally design nanoparticles for targeting specific organelles. This is important for delivering therapeutics and imaging probes to subcellular organelles (e.g., the nucleus or mitochondria) where they may be more effective or enable the study of biological processes in live cells.

The nucleus is the primary target of many chemotherapeutics, probes and small molecules for effectively treating and diagnosing diseases. Such targeting is often achieved by conjugating the nuclear localization signal (NLS) peptide to a therapeutic agent, probe, or nanoparticle. The NLS is essentially a positively-charged peptide sequence that interacts with importin proteins to actively deliver the payload to the nucleus. While the NLS has been successfully demonstrated to assist the delivery of nanoparticles into the nucleus, few studies have investigated the role of surface ligand density and nanoparticle size on nuclear transport. For example, the size of gold nanoparticles has been shown to dictate their

P. S. Tang, Prof. W. C. W. Chan
Institute of Biomaterials and Biomedical Engineering
Donnelly Center for Cellular and Biomolecular Research
Chemistry, Chemical Engineering
Materials Science and Engineering
University of Toronto
160 College St., 4th Floor, Toronto, ON, M5S 3G9, Canada
E-mail: warren.chan@utoronto.ca
Dr. S. Sathiamoorthy, Dr. I. Inamoto, Prof. J. A. Shin
Department of Chemistry
University of Toronto
3359 Mississauga Road, Mississauga, ON, L5L 1C6, Canada
L. C. Lustig, Prof. L. Z. Penn
Department of Medical Biophysics
University of Toronto
101 College Street, Room 13–706, Toronto, ON, M5G 1L7, Canada
L. C. Lustig, Dr. R. Ponzielli, Prof. L. Z. Penn
Princess Margaret Cancer Center
University Health Network
101 College Stree, Room 13-706, Toronto, ON, M5G 1L7, Canada

DOI: 10.1002/smll.201401056

NANO MICRO small

intracellular destination.[4] In the absence of NLS, nanoparticles with diameters of 5.5 nm were unable to enter the nucleus while those with diameters of 2.4 nm were found inside the nucleus. The upper limit for active nuclear transport has been demonstrated with 26 nm gold nanoparticles coated with proteins containing NLS,[9] but the specific physicochemical properties for optimal nuclear transport remain unknown. Here we used quantum dots as a model nanoparticle for assessing the effects of NLS ligand density and particle size on nuclear transport. Quantum dots are fluorescent nanoparticles that can be coated with NLS peptides and quantified in cells using techniques such as inductively-coupled plasma-atomic emission spectroscopy (ICP)[10] and flow cytometry.[11] Quantum dots have also been used as carriers for therapeutics or imaging agents to characterize and analyze intracellular processes.[12–14] Not only will using quantum dots provide a better understanding of nuclear transport, our study may also provide an additional benefit to guiding their design as nuclear probes for imaging genetic processes, or as therapeutic carriers that can interact with nuclear components.

2. Results

2.1. Design and Preparation of Quantum Dot Bioconjugates

Commercially available ZnS-capped alloyed CdSeS and ZnS-capped CdSe quantum dots were chosen for this study. Those with alloyed cores had an additional proprietary metal coating on top of the ZnS shell. These quantum dots had sizes ranging from 3.0 to 8.0 nm, and their optical properties and hydrodynamic sizes were characterized prior to use in all biological studies (**Figure 1**). CdSeS/ZnS quantum dots (diameter = 4.5 nm) were used unless otherwise specified. A NLS peptide sequence was chosen for its well established ability to deliver small drugs and nanoparticles into the nucleus.[15] A space filler peptide was used to maintain a constant surface density of total peptides. A panel of space filler peptides was tested (see Table S1 and Figure S1a in the Supporting Information). Interestingly, neither a mutated or scrambled NLS sequence was able to completely abolish nuclear transport of CdSeS/ZnS quantum dots, so they were not used in the rest of the study. The Control peptide used in this study was a random peptide sequence that showed no nuclear transport activity. Both NLS and Control peptides were coated onto CdSeS/ZnS and CdSe/ZnS quantum dot surface via poly-histidine interactions where the imidazole side chains of the histidines bind to the Zn ions.[16,17] **Figure 2**a provides a schematic of a peptide bound to a quantum dot and the linking chemistry. This self-assembly approach for coating peptides onto the quantum dot surface has been shown to be rapid (<30 min), with high affinity (equilibrium binding constant, $K_d^{-1} \approx 1 \times 10^9$ M^{-1}) and a low dissociation rate ($k_{off} < 0.001$ s^{-1}).[17] The surface valence of biomolecules on the quantum dot can be controlled by adjusting the molar ratios of peptides to quantum dots during the reaction.[18] In this study, the NLS density was manipulated by adjusting the stoichiometric ratios of NLS and Control peptides while keeping the surface density of total peptides constant (Figure 2b). We first demonstrated that the affinities of NLS and Control peptides to CdSeS/ZnS quantum dot surface were identical using a fluorescence-based protein assay (Figure 2c). We next confirmed that this approach was capable of producing quantum dots with desired NLS densities using fluorescently labeled NLS peptides. Our experiment showed a strong correlation ($R^2 = 0.9972$) between the expected and measured surface NLS densities (Figure 2d).

2.2. Cellular Interaction of Quantum Dot-NLS Bioconjugates

Previous studies have shown that nanoparticles can enter cells and the nucleus.[19] However in most of these studies, the amount of nanoparticles that entered the nucleus was not quantified. In the present work, a simple method was used to determine the number of nanoparticles in the nucleus. We isolated the nuclei from cells incubated with quantum dots using a commercial nucleus isolation kit and measured the metal content of the isolated nuclei using ICP (see Experimental Section for details). The measured metal concentration allowed for determination of the number of quantum dots. However, this technique cannot differentiate quantum dots inside the isolated nuclei from those that adsorbed onto the surface of these isolated nuclei. Therefore, confocal fluorescence microscopy was used to confirm these quantum dots were inside the isolated nuclei rather than simply adsorbed on the nuclear membrane (Figure 1d–f).

The percentage of quantum dots that entered cells and subsequently their nuclei was determined by comparing the amount of quantum dots in the nuclei to that in the whole cells. In the initial experiments, CdSeS/ZnS quantum dots were coated with cell-penetrating peptides (see Table S1 in the Supporting Information, denoted as CPP) and NLS peptides. We initially considered this design because we thought the cell-penetrating peptides would deliver the quantum dots into the cells through receptor-mediated endocytosis, escape the endo-lysosomal vesicles, and enter the cytoplasm where NLS peptides would actively transport the quantum dots into the nucleus by interacting with the importin proteins. The NLS peptides alone were found to deliver the quantum dots into the cytoplasm and then into the nucleus, while the cell-penetrating peptides alone were found 50% less efficient for nuclear transport (see Figure S1b,c in the Supporting Information). Therefore, the cell-penetrating peptides were omitted in the rest of this study, as multiple peptides were not required for nuclear delivery. Cytoplasmic delivery of CdSeS/ZnS quantum dots by the NLS peptides was likely attributable to the positive zeta potential of the quantum dots modified with these peptides (**Figure 3**). It is well-known that cationic nanoparticles can enter cells via endocytosis.[6] For example, a positively-charged Tat peptide has been shown to deliver its quantum dot bioconjugates into cytoplasm by endocytosis.[20,21] To determine whether cellular uptake of CdSeS/ZnS quantum dot-NLS bioconjugates was mediated

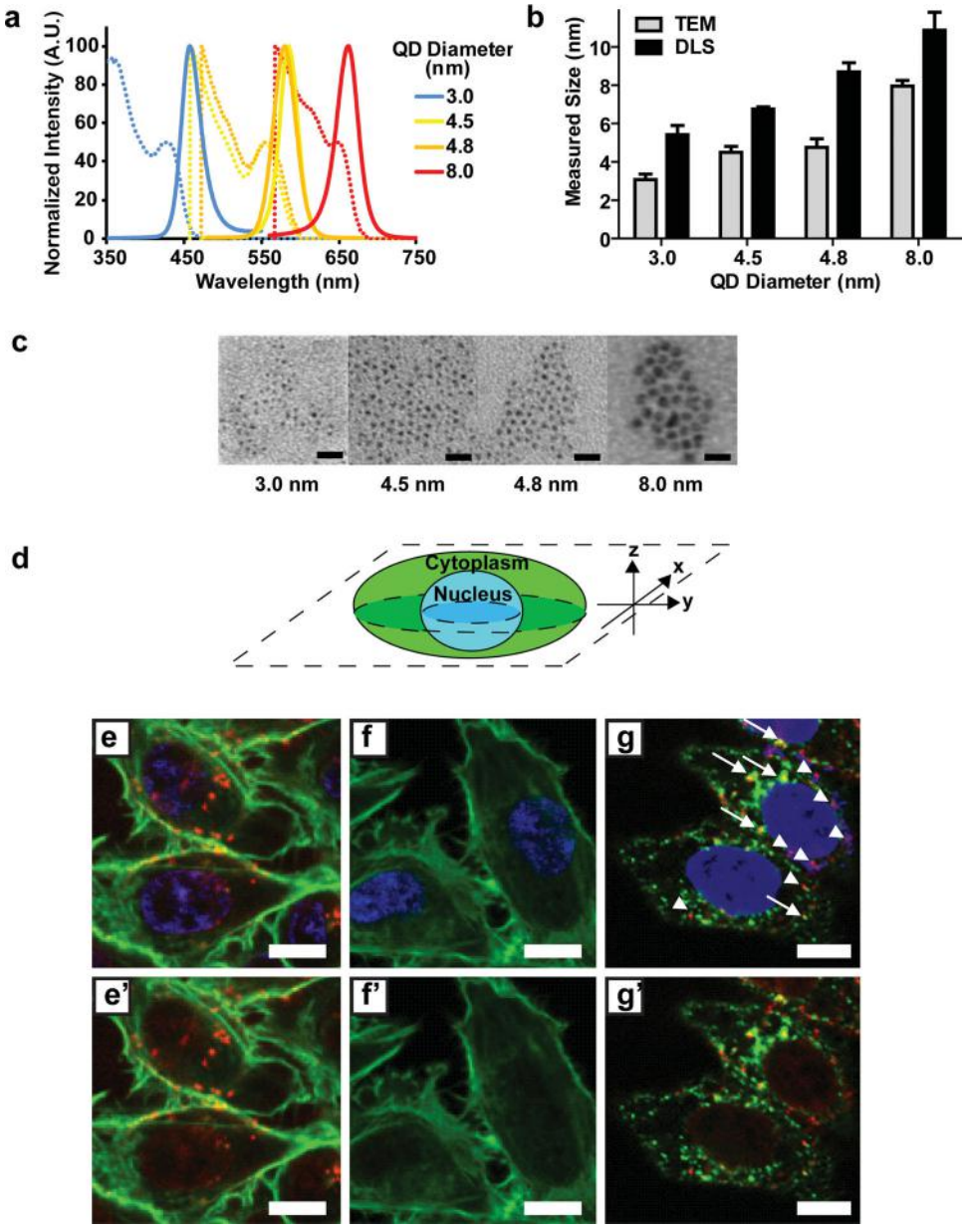

Figure 1. Characterization of quantum dots. a) Fluorescence (solid line) and absorbance (broken line) spectra of quantum dots. b) The core/shell sizes and hydrodynamic sizes of the CdSeS/ZnS and CdSe/ZnS quantum dots measured by transmission electron microscope (TEM) and dynamic light scattering (DLS). $n = 3$ which would have a total of 150 particles analyzed for each quantum dot size. c) Representative electron microscopy images for these quantum dots. These quantum dots were composed of either CdSeS/ZnS alloyed core/shell (diameter = 4.5 nm) or CdSe/ZnS core/shell (3.0, 4.8, 8.0 nm). Scale bars equal 200 nm. d) Confocal fluorescence microscopy images in the present study were cross-sections through representative cells and their nuclei as illustrated in the schematic. e) Confocal fluorescence microscopy images demonstrated nuclear transport of CdSeS/ZnS quantum dots-NLS bioconjugates, which were found mostly inside the nucleus. f) In contrast, quantum dots with the Control peptides showed minimal cellular uptake and negligible nuclear transport. Color legends: nucleus (blue), actin (green) and quantum dot (red). g) Confocal fluorescence images demonstrating the colocalization of endosome markers (green) and CdSeS/ZnS quantum dot-NLS bioconjugates (red), shown as yellow fluorescence (arrows). Arrowheads highlight red fluorescence, suggesting endosomal escape of quantum dots. These quantum dots were found mostly inside the nuclei (blue). Blue color was removed to highlight the red fluorescence from quantum dots inside the nucleus (e',f',g'). Scale bars equal 10 μm. The images were acquired with 60x UPlanApo objective (NA = 1.2) with the following Excitation (Ex) and Emission (Em) wavelengths for nuclei (λ_{ex} = 405 nm; λ_{em} = 425/50 nm), actin (λ_{ex} = 488 nm; λ_{em} = 500/100 nm) and quantum dots (λ_{ex} = 405 nm; λ_{ex} = 560 nm long-pass filter).

by endocytosis, cells were simultaneously treated with green fluorescent endosome markers (Alexa 488-tagged transferrin) and red fluorescent CdSeS/ZnS quantum dot-NLS bioconjugates. The green fluorescent Alexa tag was shown to co-localize with the red fluorescence from the CdSeS/ZnS quantum dot-NLS bioconjugates, as demonstrated by yellow colour under confocal microscopy (Figure 1g). The endosome/quantum dot complexes were mostly found in

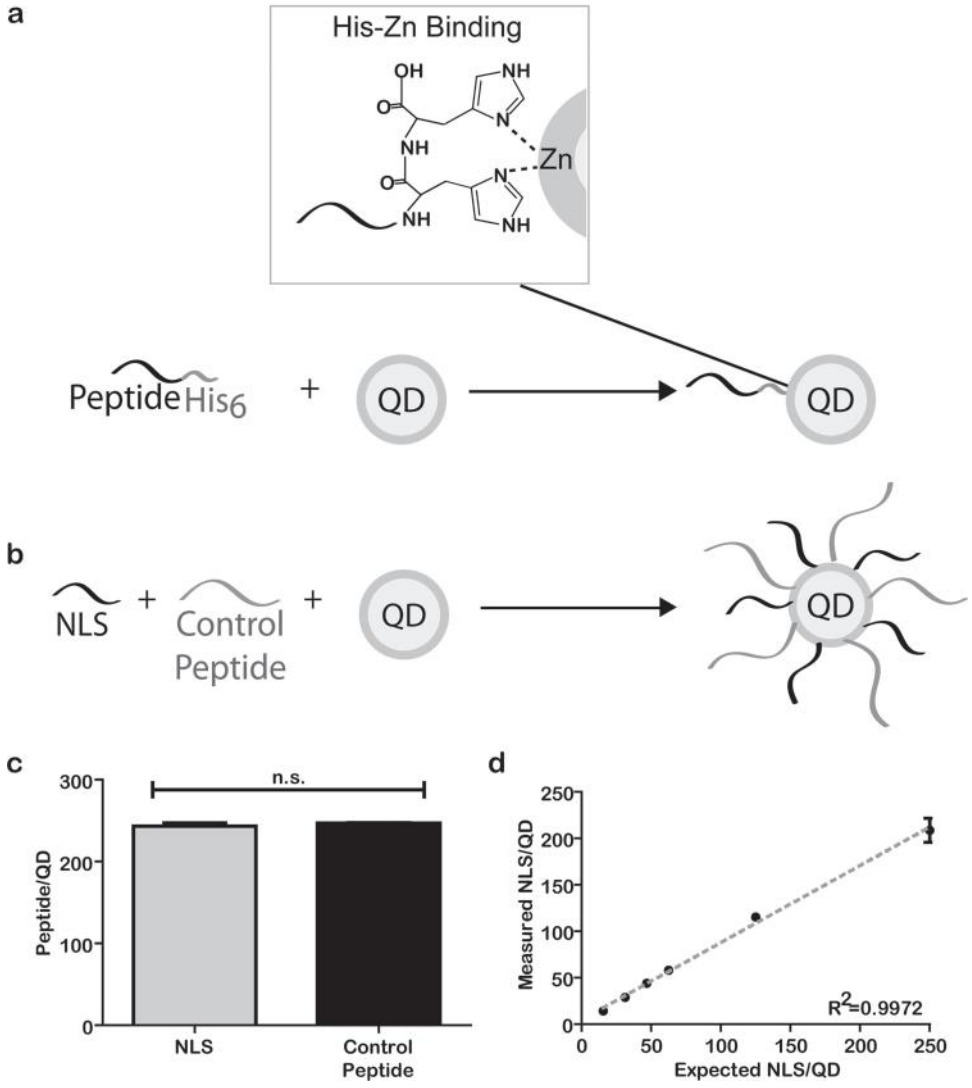

Figure 2. Engineering surface peptide densities of quantum dots. a) Schematic for peptide adsorption onto quantum dots through metal-affinity coordination between its histidine appendage (His_6) and the Zn ions on the quantum dot surface with high affinities. b) Schematic showing the peptide heterogeneity can be achieved by incubating quantum dots with nuclear localization signal peptides (NLS) and the Control peptides. The ratio of different peptides on the surface can be controlled by stoichiometry. c) The NLS and Control peptides have identical affinity between the His_6 and CdSeS/ZnS quantum dots as determined by a fluorescence-based protein assay. d) Manipulation of NLS peptide density was further confirmed by quantifying fluorescently labeled NLS peptides on CdSeS/ZnS quantum dot surface in the presence of the Control peptides. Broken line: linear regression. The total peptide (NLS + Control peptide) number per quantum dot was kept at 250, so the expected NLS/quantum dot ratios between 15.625 and 250 correspond to NLS densities between 6.25% and 100%. n.s., not statistically significant; $n = 3$.

the perinuclear area. Such perinuclear accumulation of the CdSeS/ZnS quantum dot-loaded vesicles has been previously reported for quantum dot-Tat peptide bioconjugates because the bioconjugates were trapped inside vesicles for up to 24 h.[20] In contrast, the CdSeS/ZnS quantum dot-NLS bioconjugates were capable of endosomal escape as evidenced by red quantum dot fluorescence observed outside the endosomes (Figure 1g). These escaped quantum dot-NLS bioconjugates were capable of subsequent nuclear transport as illustrated by their red fluorescence inside the nucleus (Figure 1g'), which was more diffused and dimmer compared to their counterpart inside endosomes. The diffusion pattern suggested that these CdSeS/ZnS quantum dots remained dispersed after endosomal escape and likely entered the nucleus as single nanoparticles.

2.3. Effects of Ligand Density on Nuclear Transport of Quantum Dots

To examine the effect of the ligand density on nuclear transport, CdSeS/ZnS quantum dots were prepared with seven ligand densities: 0, 6.25, 12.5, 18.75, 25, 50 and 100% NLS. The quantum dot surface peptide density was kept constant with space filler peptides as illustrated earlier (Figure 2). Cells were incubated with the CdSeS/ZnS quantum dot-

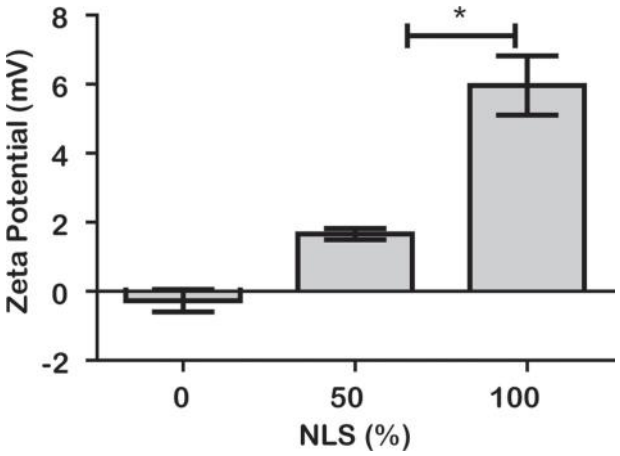

Figure 3. Zeta potential of quantum dot-NLS bioconjugates. The average zeta potential values were 0, +2, and +6 mV for CdSeS/ZnS quantum dots with 0%, 50% and 100% NLS densities, respectively, $*p < 0.05$; $n = 3$.

NLS bioconjugates for 1 h, washed thoroughly, collected, and analyzed by ICP. The results are described in **Figure 4**a,b. For these results to be comparable across all NLS densities, we defined "nuclear transport" as following:

$$\text{Nuclear transport} = \frac{\text{Quantity of nuclear quantum dots}}{\text{Quantity of intracellular quantum dots}}$$

This value, expressed as a percentage, would account for different cellular uptake efficiencies of these quantum dots with various NLS densities. The present study showed a drastic and linear increase in nuclear transport with NLS densities up to 20% (R^2 = 0.9276), at which approximately half of total intracellular CdSeS/ZnS quantum dots were transported into the nucleus (Figure 4c). Any increase above 20% NLS density only resulted in a modest increase in nuclear transport, and deviation from the initial linear relationship between NLS density and nuclear transport. These CdSeS/ZnS quantum dot-NLS bioconjugates were capable of nuclear transport up to 2 h post treatment, and their nuclear transport reached a plateau at 30 min (see Figure S2 in the Supporting Information). To confirm nuclear transport of CdSeS/ZnS quantum dots, we used microinjection to deliver these quantum dot-peptide bioconjugates into the cytoplasm, followed by assessment of their nuclear transport based on their fluorescence. Cells were first microinjected with the green co-injection marker fluorescein isothiocyanate (FITC)-tagged dextran (which labels the initial injection site) and red emitting CdSeS/ZnS quantum dot-NLS bioconjugates, and analyzed using confocal fluorescence microscopy. This co-injection marker does not passively diffuse across the nuclear membrane[22] and is used here to identify cells that received microinjection into the cytoplasm. Representative frames of videos for quantum dot-bioconjugates of NLS and Control peptides at indicated time points are shown (**Figure 5**, and see Supporting Information for these videos). Image analysis demonstrated that nuclear transport of cytoplasmic CdSeS/ZnS quantum dots was enabled by the NLS peptides, but not

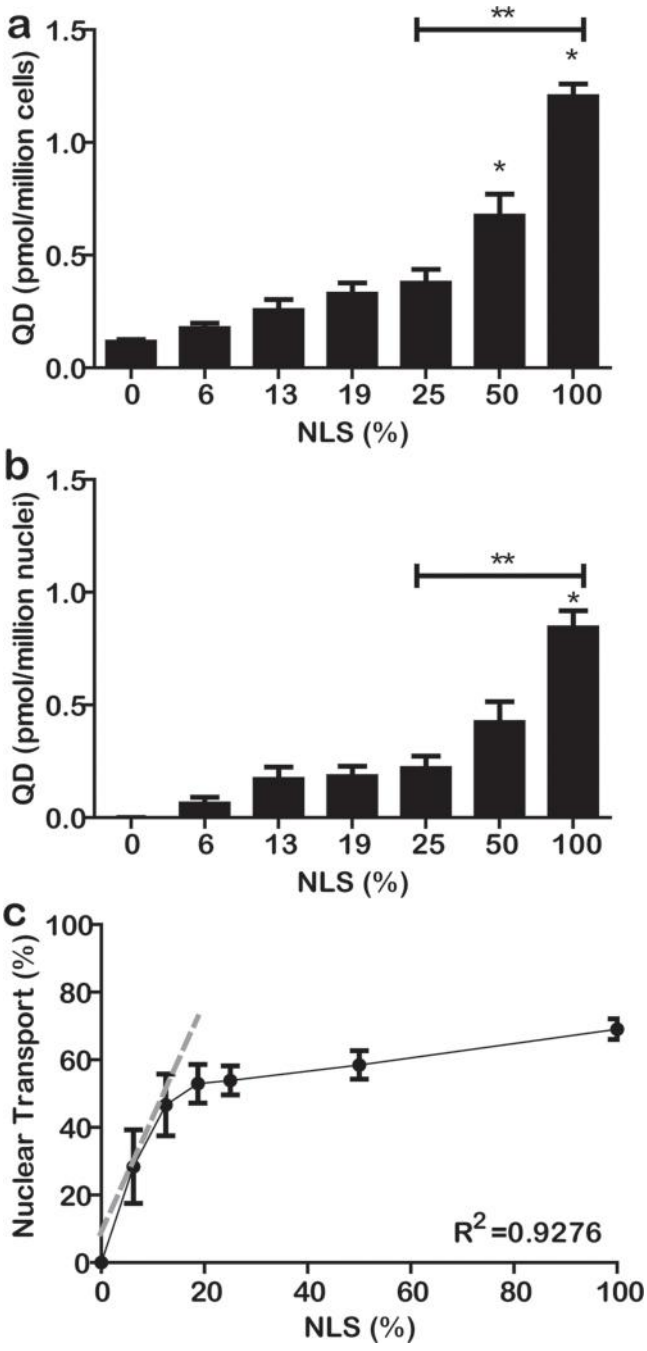

Figure 4. Effects of NLS density on cellular uptake and nuclear transport. Cells were incubated with CdSeS/ZnS quantum dot-peptide bioconjugates of indicated NLS densities for 1 hour, trypsinized, and collected for ICP analysis. We present results for a) the cellular uptake of quantum dots with different densities of NLS and b) their respective nuclear accumulation. $*p < 0.05$ compared to the next lower NLS density; $**p < 0.05$; $n = 3$. c) Nuclear transport was expressed as the ratio of nuclear quantum dots to intracellular quantum dots in percentage to account for different cellular uptake efficiencies of quantum dots with various NLS densities. The NLS density effect on nuclear transport showed a steep increase up to approximately 20% NLS followed by a plateau. Broken line: linear regression, R^2: correlation coefficient; $n = 3$.

the Control peptide (Figure 5b). These results also confirmed the ICP results that the measured nuclear transport of CdSeS/ZnS quantum dots was attributable to their presence

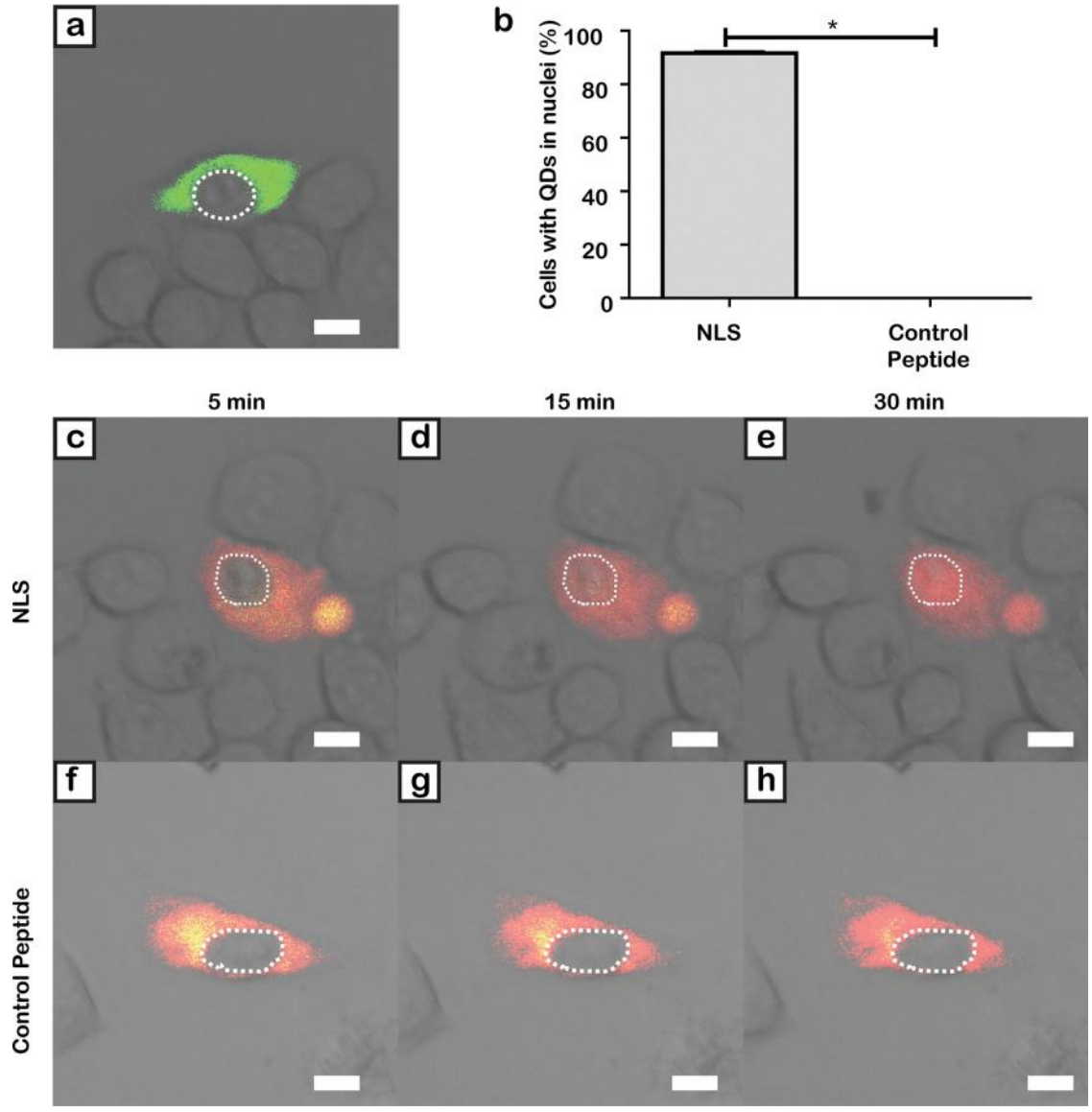

Figure 5. Nuclear transport of cytoplasmic quantum dot–peptide bioconjugates. Green emitting FITC-Dextran (72kDa) was mixed with red emitting CdSeS/ZnS quantum dot-peptide bioconjugates and microinjected into cells (which appeared orange). a) FITC-Dextran does not enter the nucleus. In these experiments, the monitoring of the green fluorescence of the cell will determine if the quantum dots are accidentally microinjected into the nucleus. If such a case occurred, we would discard the cells for quantitative analysis. b) Representative images were quantified as the ratio of the number of cells with nuclear accumulation of quantum dot at 30 min post injection. Once injected, these cells were imaged using confocal fluorescence microscopy from 5 to 30 min post injection (see Supporting Information for representative videos). At 5 min, fluorescence resided in the cytoplasm, suggesting successful microinjection (c,f). NLS peptides facilitated nuclear transport of quantum dots over time (c–e) whereas, in contrast, the Control peptide did not (f–h). This was observed up to 2 hours post injection (data not shown). The white dashed lines highlight the nuclear-cytoplasmic boundary. Scale bars equal 10 μm. The images were acquired with 60× UPlanApo water objective (NA = 1.2) with indicated Excitation (Ex) and Emission (Em) wavelengths for nuclei (λ_{ex} = 405 nm; λ_{em} = 425/50 nm), FITC-Dextran (λ_{ex} = 488 nm; λ_{em} = 500/100 nm) and quantum dots (λ_{ex} = 405 nm; λ_{ex} = 560 nm long-pass filter). $^{**}p < 0.01$; $n = 3$ with 30 cells analyzed per peptide.

inside the nucleus, and not due to their non-specific binding to the surface of the nucleus.

2.4. Effects of Particle Size on Nuclear Transport of Quantum Dots

A second set of quantum dots made of CdSe cores and coated with an inorganic ZnS shell were used for the subsequent size effect studies as the fluorescence of the CdSeS/ZnS alloyed quantum dots are tuned by composition and not by size. Three sizes (3.0, 4.8, 8.0 nm) were chosen to investigate the effects of particle size on nuclear transport. Cells were treated with these CdSe/ZnS quantum dots for 1 h before cell collection and nucleus isolation for ICP analysis. In the absence of NLS, cellular uptake was seen in all three sizes of quantum dots and was the highest for the 4.8 nm CdSe/ZnS quantum dots (**Figure 6**a), but nuclear accumulation was only seen in the 3.0 nm CdSe/ZnS quantum dots (Figure 6b,c). Since the NLS was absent, the observed nuclear accumulation can be

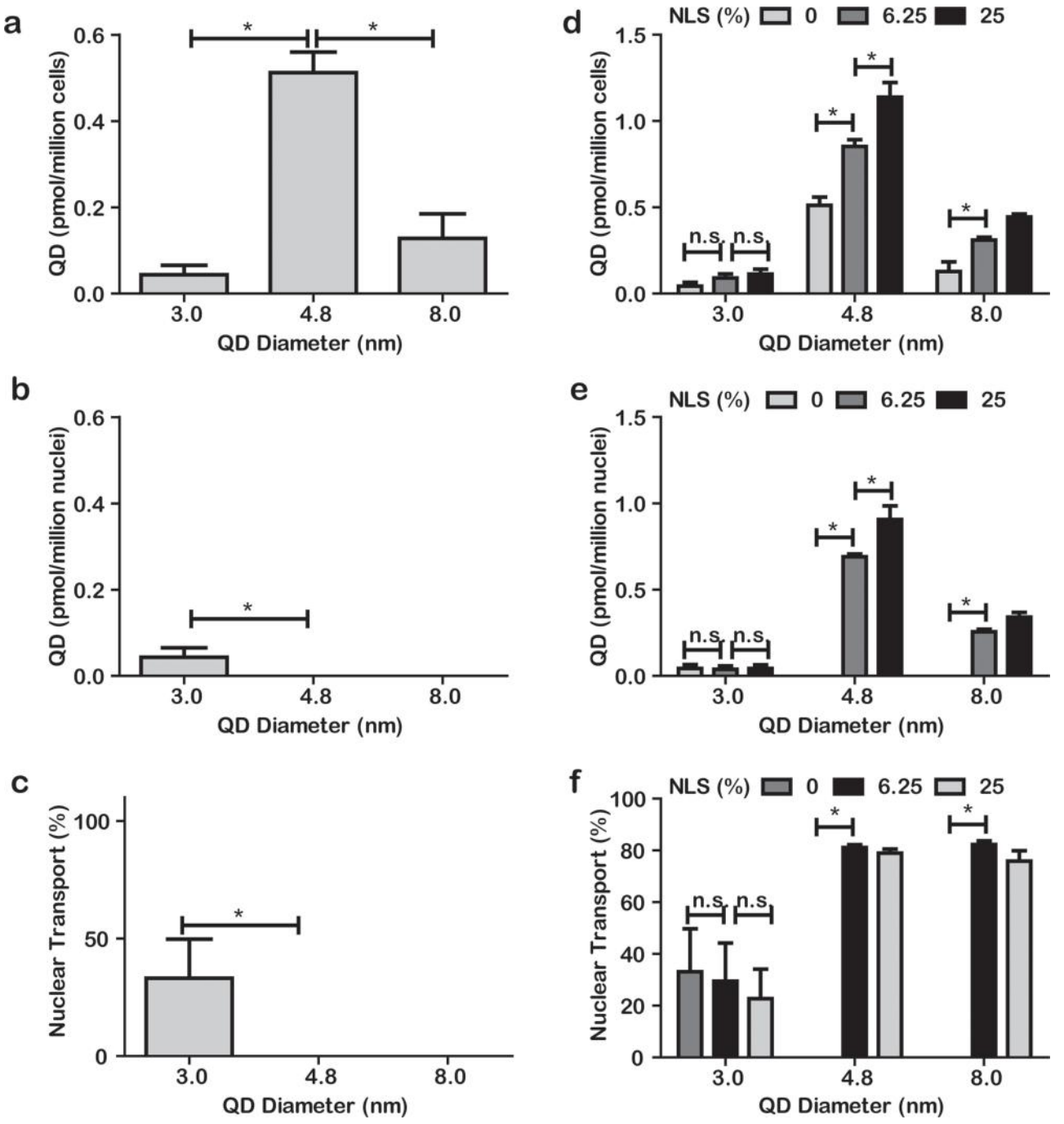

Figure 6. Effects of particle size on NLS-dependent nuclear transport. Three sizes of CdSe/ZnS quantum dots (diameters = 3.0, 4.8, 8.0 nm) were used to study the size effects on NLS-dependent nuclear transport. Cells were treated with quantum dot-peptide bioconjugates with indicated sizes and NLS densities for 1 hour before collection for ICP analysis. a) The particle size effects were first determined using three sizes of quantum dots with 0% NLS, showing optimal size of 4.8 nm for NLS-independent cellular uptake. b) NLS-independent nuclear accumulation was only seen for the smallest 3.0 nm quantum dots. c) A similar trend was seen for nuclear transport of the quantum dots. d–f) The NLS density effects on each size of quantum dots' d) cellular uptake, e) nuclear accumulation, and f) nuclear transport were determined. *$p < 0.05$; n.s., not statistically significant; $n = 3$.

attributed to passive diffusion of these small 3.0 nm CdSe/ZnS quantum dots. In contrast, NLS-independent passive diffusion was not seen for the larger 4.8 and 8.0 nm CdSe/ZnS quantum dots, suggesting an upper size limit between 3.0 and 4.8 nm for nuclear entry via a passive diffusion mechanism. The presence of NLS enhanced the cellular uptake and appeared to facilitate the nuclear accumulation of the 4.8 and 8.0 nm CdSe/ZnS quantum dots (Figure 6d–f), but higher NLS densities did not further increase the percentage of CdSe/ZnS quantum dots transported into the nucleus from the cytoplasm. In our ligand density effect study above, a NLS density plateau was also seen for the 4.5 nm CdSeS/ZnS

NANO MICRO small

quantum dots, above which NLS density had minimal effects on nuclear transport, suggesting the observed effects were not specific to the 4.5 nm CdSeS/ZnS quantum dots.

2.5. Cytotoxicity of Intracellular Quantum Dots

The CdSeS/ZnS quantum dot bioconjugates had no effects on cell viability during the nuclear transport study, or up to 72 h post treatment (see Figure S3 in the Supporting Information). The ZnS shell has been demonstrated to render CdSe quantum dots minimally cytotoxic.[23] This suggests that the cells remained physiologically viable in the presence of the CdSeS/ZnS and CdSe/ZnS quantum dots, and the observed effects on nuclear transport were indeed attributable to their design parameters, such as ligand density and particle size, not cytotoxic effects. A parallel study demonstrated minimal exocytosis of these intracellular CdSeS/ZnS quantum dot-NLS bioconjugates over time (see Figure S4 in the Supporting Information) and that they were retained in the cells, which is consistent with previous work.[24] Previous studies investigated three areas of cellular interaction with nanoparticles—cellular uptake,[25] mitotic partitioning,[26] and cell tracking[13]—and established that the internalized nanoparticles remain inside cells and are transferred to daughter cells when parent cells divide.

3. Discussion

Earlier studies on nuclear-targeting nanoparticles provided proof of concept for nuclear transport, but these studies did not correlate the nuclear transport process and the nanoparticles physicochemical properties, such as ligand density and particle size. The effects of these parameters have been mainly reported on cellular uptake of nanoparticles.[2,4,27] Studies on nuclear transport are often qualitative and require physical methods such as microinjection or electroporation to facilitate cellular delivery of NLS-quantum dot bioconjugates.[28,29] Gerion et al. published one of the first studies on nuclear transport of silanized CdSe/ZnS quantum dots coated with NLS peptides.[28] They showed that 15% of their CdSe/ZnS quantum dots entered the nucleus while the other 85% were in the perinuclear space. They rationalized that the nuclear pore size, shape, and permeability might change during a cell's life cycle, and subsequently alter the size limit for nuclear transport of quantum dots. In 2004, techniques to characterize nanoparticle physicochemical properties were in early development and, hence, it was logical to assume the biological system was responsible for the differential uptake. Our results complement the Gerion et al. finding and suggest that the quantum dot physicochemical properties are also important in mediating nuclear transport. Likely, the defined physicochemical properties for optimal uptake are related to properties of both the particles and the nuclear pores.

Our present work contributes to this research topic by demonstrating a facile method to manipulate the ligand density, systemic investigation of the effects of ligand density and particle size on nuclear transport, and development of a quantitative method to measure nanoparticles in the nucleus. These design parameters included seven ligand densities and three nanoparticle sizes, and the results further refined the upper size limit for NLS-independent nuclear entry through nuclear pore complexes. Additionally, we show a direct correlation of NLS ligand density with cellular uptake and nuclear accumulation (Figure 4a,b). The effects on nuclear transport were more profound below 20% NLS density, above which the effects became moderate. This could be attributed to the rate limitation of the active nuclear transport process with two major phases: 1) recognition of NLS-tagged cargos by adaptor proteins (importin α and β) and 2) the passage of this tripartite complex through the nuclear pore complex.[30] While the recognition phase might be facilitated by the presence of more NLS, the passage phase is limited by the physical dimensions of the nuclear pore complex.[31] The increased nuclear transport might also be attributed to the rate of endosomal escape, which has been previously reported to be the rate-limiting step for nuclear delivery by nanoparticles.[32] The NLS peptide used in the current study is rich in amino acids that have been shown to facilitate endosomal escape. There are 11 such amino acids (lysine, arginine, and histidine) in this NLS peptide of 16 amino acids. Both arginine and lysine facilitate endosomal escape of nanoparticles through fusion with endosomal membranes.[33] On the other hand, histidine facilitates endosomal escape through its imidazole ring (pK_{a3} = 6.04) which increases the buffering capacity in endosomes and lysosomes.[34] Poly-histidine appendage with as few as 4 histidines is sufficient to serve as a linker between peptides and quantum dots.[18] Poly-histidine appendage used in the current work contains 6 histidines, and it is possible that the imidazole rings of these 2 additional residues were not involved in quantum dot binding but rather in facilitating endosomal escape. Further investigation is required to assess the effects of ligand density on each of these steps, in particular during endosomal escape and nuclear entry. We anticipate the results to be applicable to other nanoparticles, such as gold nanoparticles, which can be similarly modified with peptide ligands through poly-histidine-mediated self assembly.[35]

In addition to the ligand density, the size of the quantum dots also plays an important role in nuclear transport. The double-layered nuclear envelope presents a barrier to entry into the nucleus. Nuclear pore complexes control the transport process, and actively transport gold nanoparticles up to 26 nm in size,[9] and allow for passive diffusion of smaller nanoparticles in the absence of NLS. There is a discrepancy for the upper limit for passive diffusion (5.2 nm or 9.0 nm) because non-metallic probes, such as dextrans[36] and protein probes,[37] respectively, were used as the delivery vehicle in these studies. In a previous study, quantum dots with diameters between 2.1 and 4.4 nm were used to investigate the upper limit for passive diffusion of metallic nanoparticles across nuclear pore complexes, and the limit was found to be approximately 3.1 nm.[38] However, cells were fixed and permeabilized prior to incubation with quantum dots, so it is unclear whether this limit can also be observed in live cells. In contrast, the present study demonstrates the size limit to be approximately 3.0–4.8 nm in live cells, based on the direct

assessment of the physical sizes of the nanoparticles (Figure 1c). NLS is required for nuclear transport of quantum dots that are larger than this size. In the presence of NLS, the 4.8 nm quantum dots demonstrated the highest cellular uptake and nuclear accumulation (Figure 6d,e). Size alone was insufficient to explain this phenomenon because this optimal size was an intermediate one between 3.0 and 8.0 nm. Rather it should be attributable to the balance between NLS-dependent transport and nuclear retention. For nanoparticles > 20 nm, an increase in size led to slower diffusion in the cytoplasm to reach the nuclear pore complex, which subsequently resulted in less nuclear transport and lower nuclear retention.[9] On the other hand, smaller protein constructs with a physical size less than 3 nm in one cross-section are capable of diffusing from the nucleus back to the cytoplasm, which reduced their nuclear retention. An addition to their length reduces this diffusion, maintains their nuclear retention, and subsequently increases nuclear accumulation.[39] In support, the present study demonstrates NLS-independent nuclear entry of the 3.0 nm quantum dots. Other factors—such as surface curvature, which is a function of particle sizes—have been reported to influence the binding affinity of ligands on these particles.[40] These factors cannot be excluded from this present study.

While our study clearly demonstrates the effects of particle size and ligand density on cellular uptake and nuclear transport, we did not consider the length difference between the Control peptide and the native NLS peptide, or the effect of peptide length on nuclear transport. We attempted to use scrambled and mutated NLS peptides of similar lengths to the native NLS peptides but both scrambled and mutated NLS peptides were incapable of inhibiting nuclear delivery of quantum dots. Based on these early results, we were mostly concerned about finding peptides that can coat the surface of the quantum dots and completely abolish their nuclear transport. With our Control peptide, we cannot exclude the influence of its length on interfering with the NLS-mediated nuclear transport process of quantum dots. The longer length of the Control peptide may block the interaction of the NLS peptide with the importin proteins in an active transport process. We recently showed that the polymer polyethylene glycol could fill the space between herceptin antibodies on the nanoparticle surface. If the polyethylene glycol is too long, it can negatively influence the herceptin targeting specificity to cell receptor.[41] Identification of optimal filler peptides is challenging, as any change in the length of peptides could alter their isoelectric point, hydrophobicity, and functional groups. These changes in chemical properties could affect how they are coated on the quantum dots as well as the nanoparticle stability and overall surface charge. Future work is needed to identify proper filler peptides as well as to study the effect of peptide coating heterogeneity on cellular uptake and subcellular transport.

4. Conclusion

In summary, the present work demonstrates the effects of design parameters on the nuclear transport of nanoparticles, using a strategy designed for facile manipulation of these parameters. Our future work will assess the effects of other design parameters and the intra-parameter relationships. Knowledge of their effects and relationships will facilitate development of nuclear-targeting carriers.

5. Experimental Section

Preparation of Water-Soluble Quantum Dots: Chemicals were purchased from Sigma-Aldrich unless otherwise specified and used without further purification unless otherwise indicated. CdSeS/ZnS alloyed core/shell quantum dots were purchased from Cytodiagnostics (emission peak wavelength at 575 nm with a diameter of 4.5 nm) and CdSe/ZnS core/shell quantum dots from Ocean NanoTech (emission peak wavelengths at 450, 575, 665 nm for diameters of 3.0, 4.8, 8.0 nm, respectively). These organic quantum dots were rendered water-soluble by 4 h of ligand exchange with mercaptoacetic acid as previously described,[42] and purified as following. In a typical preparation, quantum dot solution (500 uL) was added to acetone (500 uL) containing aqueous solution (40 uL) of tetramethylammonium hydroxide (25% w/w), which was included to facilitate phase transfer of water-soluble quantum dots from the organic phase to the aqueous phase. Excess mercaptoacetic acid was removed by centrifugation (1000 *g*, 5 min) and disposal of the supernatant. The process was repeated another 2 times with acetone (1 mL). Trace acetone was left to completely dry before the quantum dot pellet was re-dispersed in phosphate-buffered saline, adjusted to pH 7.4, filtered through 0.22 μm syringe filter, and stored at 4°C before use.

Characterization of Quantum Dot-Peptide Bioconjugates: Absorbance and fluorescence spectra were measured using a UV-1601 spectrophotometer (Shimadzu) and a FluoroMax-3 fluorimeter (Jobin Yvon Horiba), respectively. Quantum dot concentrations were determined by absorbance at the first excitonic peak using extinction coefficients provided by the manufacturers. The diameters of quantum dots were determined by Tecnai-20 electron microscopy (FEI) using carbon film coated copper grids (300 mesh, Ted Pella Inc.), and at least 50 nanoparticles were measured for each sample. Hydrodynamic diameters of these quantum dots were measured by dynamic light scattering on a Nano ZS Zetasizer (Malvern) with a 633 nm laser. Zeta potential values of these quantum dot bioconjugates (20 nM) were also measured using this Nano ZS Zetasizer, but in HEPES buffer (10 mM; final pH 7.5). The DIP-CELL electrode was cleaned between each measurement by bach sonication. Each sample was limited to 10 runs of measurement to minimize potential damages of the electrical current to the quantum dot bioconjugates. Both hydrodynamic diameters and zeta potentials were presented as the average number from at least 3 batches of preparation.

Preparation of Quantum Dot-Peptide Bioconjugates: Water-soluble quantum dots were further stabilized with 1 kDa methoxy-polyethylene glycol-sulfhydryl (mPEG-SH; CreativePEGWorks) through ligand exchange (60 °C, 1 h) in 25 mM borate buffer (pH 8.3), followed by removal of excess PEG with Amicon Ultra Centrifugal Filters (Molecular Weight Cut-off: 30 kDa; Millipore). The process was repeated another 2 times with pure water. Custom peptides were synthesized by Biomatik. Peptide adsorption was carried out in the same borate buffer (37 °C, 1 h) with a constant surface density of total peptides (NLS and Control peptide), which

NANO MICRO small

was 250 for the 4.5 nm quantum dots, and adjusted accordingly for other sizes of quantum dots to account for their different surface areas. Successful PEGylation and peptide adsorption were confirmed with agarose gel (0.7%) electrophoresis (15 min, 135 V) in Tris/borate/EDTA buffer (0.5X) and imaged with a Typhoon Trio variable mode imager (GE Healthcare). Peptide adsorption onto quantum dots was quantified by a depletion assay after removing excess, unbound peptides from quantum dot-peptide bioconjugates with a tabletop ultracentrifuge (Beckman Optima MAX-XP), as previously described.[43] In brief, quantum dot-peptide bioconjugates were removed from the supernatant by ultracentrifugation (200 000*g*, 60 min) and confirmed by UV–Vis spectrophotometry. Proper controls were included to account for peptide loss due to ultracentrifugation. The remaining peptides in the supernatant were quantified by a fluorescence-based protein assay using a FluoroProfile Protein Quantification Kit (Sigma) according to the manual. Alternatively, a custom FITC-labeled NLS peptide (Biomatik) was used and quantified by a calibration curve of known FITC-labeled NLS peptide concentrations.

Cellular Uptake of Quantum Dots: HeLa cells (ATCC CCL-2) were cultured and assayed as described earlier.[43] Cells were seeded at 5×10^4 cells/well into 8-well chambered cover glass slides (Nunc), or at 10^6 into 6-well plates (Nunc) for microscopic imaging and ICP quantification, respectively, and then incubated overnight to allow for cell attachment before treatment with the indicated quantum dot-peptide bioconjugates. These cells were washed thoroughly with phosphate buffered saline (1X) containing Mg^{2+} and Ca^{2+} to remove extracellular quantum dots. Intracellular quantum dots were visualized with counterstaining and controls using the FluoView 1000 laser scanning confocal microscope (Olympus).[43] Intracellular quantum dots were quantified by ICP using the Optima 7300V system (PerkinElmer) after acid digestion in HNO_3 (70 °C, 1 h).[10] Quantum dot concentrations were converted from measured Cd concentrations using Cd-quantum dot calibration curves established for each quantum dot size. Cell numbers were converted from measured Mg^{2+} concentrations using Mg^{2+} calibration curves with known numbers of cells using the technique developed by Albanese et al.[44] The effects of intracellular quantum dots on cell viability were determined by the Cell Proliferation Kit II (Roche Applied Science). Their values were expressed as percentage cell viability of non-treated cells with identical culture conditions. For endocytosis experiments, human holo-Transferrin (Sigma) was labeled with an Alexa Fluor 488 Protein Labeling Kit (Life Technologies) according to manufacturer's specifications.

Nuclear Accumulation of Quantum Dots: Nuclei of the quantum dot-incubated cells were isolated using the Nuclei EZ Prep kit from Sigma. The nuclear isolation procedures were validated as following. Isolated nuclei were stained with Hoescht 33342 and Alexa Fluor 488 phalloidin (Life Technologies) for nuclear and actin labeling, respectively. Confocal fluorescence microscopy showed only stains for the nucleus, but not actins, which are the major component of the cytoskeleton, suggesting that the collected samples contained isolated nuclei without cytosolic components. Confocal fluorescence microscopy also demonstrated that the washing protocol removed loosely bound quantum dots on the nuclear membrane, and confirmed the presence of quantum dots inside these isolated nuclei, which were subsequently quantified using ICP as described above.

Cytoplasmic Microinjection of Quantum Dot-Peptide Bioconjugates: Microinjection studies were carried out as previously described.[22] HeLa cells were seeded at 10^5 cells per 50 mm PELCO clear wall glass bottom dishes (Ted Pella Inc.), and then incubated to allow for optimal cell morphology for microinjection with solution containing quantum dot-peptide bioconjugates and a co-injection marker (FITC-tagged 72kDa Dextran; Sigma). The solution was microinjected using an Eppendorf Micromanipulator 5171 combined with an Eppendorf Transjector 5246 mounted on a Nikon TE2000 inverted fluorescence microscope. After microinjection (time 0 h), cells were imaged under the FluoView 1000 confocal microscope at the indicated time points. During live cell imaging, these cells were maintained at controlled temperature (37 °C) and CO_2 level (5%). Microinjection began with the following settings: the pressure of injection (150 hPa), time of injection (0.5 s) and the compensation background pressure (30 hPa) for comparable injection volumes between experiments. These settings need to be adjusted to accommodate variations in microneedle opening sizes, so injection volumes cannot be accurately quantified. Therefore, translocation of quantum dot-peptide bioconjugates from the cytoplasm to the nucleus was compared qualitatively. First, cells with successful microinjection into the cytoplasm, as demonstrated by clear cytoplasmic distribution of the green FITC-Dextran marker, were counted (N_1). Other cells with this marker inside the nucleus were excluded from analysis. Cells with translocation of cytoplasmic quantum dots into the nucleus, as demonstrated by quantum dot fluorescence in the nucleus, were then quantified (N_2) and expressed as the percentage of cells capable of translocating cytoplasmic quantum dots into the nucleus (N_2/N_1). At least 10 cells were analyzed per measurement.

Statistics: Unless otherwise specified, data shown are mean ± standard error results from n independent experiments ($n \geqq 3$). Statistical comparison using ANOVA and Tukey's post-hoc analysis was determined by Prism 5 software (GraphPad).

Supporting Information

Supporting Information is available from the Wiley Online Library or from the author.

Acknowledgements

All investigators acknowledge the Canadian Health Research Program (CHRPJ 385829 and CPG-104290) for financial support. The authors acknowledge the Canadian Institute of Health Research (MOP-93532; G118160781), Natural Sciences and Engineering Research Council of Canada (NETGP 35015–07, RGPIN 288231–09 and 203312–08), Canadian Research Chairs Program (950–203403), Canadian Foundation for Innovation, and Ontario Ministry of Research and Innovation for funding support. P.S.T. would like to acknowledge the Queen Elizabeth II Graduate Scholarships in Science and Technology (Canada), Ontario Graduate Scholarships (Canada) and the International Graduate Scholarships (Taiwan). L.C.L. would like to acknowledge Natural Sciences and

Engineering Research Council of Canada for graduate scholarship. The authors also acknowledge Dr. Rodrigo Fernandez-Gonzalez for his insightful discussion of microinjection experiments, Dr. Antonia DeJong for her technical support, and Edward A. Sykes for his insightful discussion.

[1] A. Albanese, P. S. Tang, W. C. W. Chan, *Annu. Rev. Biomed. Eng.* **2012**, *14*, 1.
[2] E. Moradi, D. Vllasaliu, M. Garnett, F. Falcone, S. Stolnik, *RSC Adv.* **2012**, *2*, 3025.
[3] L. Y. T. Chou, K. Zagorovsky, W. C. W. Chan, *Nat. Nanotechnol.* **2014**, *9*, 148.
[4] E. Oh, J. B. Delehanty, K. E. Sapsford, K. Susumu, R. Goswami, J. B. Blanco-Canosa, P. E. Dawson, J. Granek, M. Shoff, Q. Zhang, P. L. Goering, A. Huston, I. L. Medintz, *ACS Nano* **2011**, *5*, 6434.
[5] A. Albanese, C. D. Walkey, J. B. Olsen, H. Guo, A. Emili, W. C. W. Chan, *ACS Nano* **2014**, *8*, 5515.
[6] S. J. Tan, N. R. Jana, S. Gao, P. K. Patra, J. Y. Ying, *Chem. Mater.* **2010**, *22*, 2239.
[7] K. Boeneman, J. B. Delehanty, J. B. Blanco-Canosa, K. Susumu, M. H. Stewart, E. Oh, A. L. Huston, G. Dawson, S. Ingale, R. Walters, M. Domowicz, J. R. Deschamps, W. R. Algar, S. Dimaggio, J. Manono, C. M. Spillmann, D. Thompson, T. L. Jennings, P. E. Dawson, I. L. Medintz, *ACS Nano* **2013**, *7*, 3778.
[8] A. H. van Asbeck, A. Beyerle, H. McNeill, P. H. M. Bovee-Geurts, S. Lindberg, W. P. R. Verdurmen, M. Hällbrink, U. Langel, O. Heidenreich, R. Brock, *ACS Nano* **2013**, *7*, 3797.
[9] N. Panté, M. Kann, *Mol. Biol. Cell* **2002**, *13*, 425.
[10] H. C. Fischer, S. Fournier-Bidoz, K. S. Pang, W. C. W. Chan, *Nanobiotechnology* **2007**, *3*, 46.
[11] L. W. Zhang, N. A. Monteiro-Riviere, *Toxicol. Sci.* **2009**, *110*, 138.
[12] X. Michalet, F. F. Pinaud, L. A. Bentolila, J. M. Tsay, S. Doose, J. J. Li, G. Sundaresan, A. M. Wu, S. S. Gambhir, S. Weiss, *Science* **2005**, *307*, 538.
[13] I. L. Medintz, H. T. Uyeda, E. R. Goldman, H. Mattoussi, *Nat. Mater.* **2005**, *4*, 435.
[14] A. M. Derfus, A. A. Chen, D.-H. Min, E. Ruoslahti, S. N. Bhatia, *Bioconjug. Chem.* **2007**, *18*, 1391.
[15] R. Misra, S. K. Sahoo, *Eur. J. Pharm. Sci.* **2010**, *39*, 152.
[16] M. Zhou, I. Ghosh, *Pept. Sci.* **2007**, *88*, 325.
[17] K. E. Sapsford, T. Pons, I. L. Medintz, S. Higashiya, F. M. Brunel, P. E. Dawson, H. Mattoussi, *J. Phys. Chem. C* **2007**, *111*, 11528.
[18] D. E. Prasuhn, J. R. Deschamps, K. Susumu, M. H. Stewart, K. Boeneman, J. B. Blanco-Canosa, P. E. Dawson, I. L. Medintz, *Small* **2010**, *6*, 555.
[19] A. G. Tkachenko, H. Xie, D. Coleman, W. Glomm, J. Ryan, M. F. Anderson, S. Franzen, D. L. Feldheim, *J. Am. Chem. Soc.* **2003**, *125*, 4700.
[20] G. Ruan, A. Agrawal, A. I. Marcus, S. Nie, *J. Am. Chem. Soc.* **2007**, *129*, 14759.
[21] J. B. Delehanty, C. E. Bradburne, K. Boeneman, K. Susumu, D. Farrell, B. C. Mei, J. B. Blanco-Canosa, G. Dawson, P. E. Dawson, H. Mattoussi, I. L. Medintz, *Integr. Biol.* **2010**, *2*, 265.
[22] J. M. Featherstone, A. G. Speers, B. A. Lwaleed, M. C. Hayes, A. J. Cooper, B. R. Birch, *BJU Int.* **2005**, *95*, 1091.
[23] A. M. Derfus, W. C. W. Chan, S. N. Bhatia, *Nano Lett.* **2004**, *4*, 11.
[24] H. C. Fischer, T. S. Hauck, A. Gómez-Aristizábal, W. C. W. Chan, *Adv. Mater.* **2010**, *22*, 2520.
[25] J. A. Kim, C. Åberg, A. Salvati, K. A. Dawson, *Nat. Nanotechnol.* **2012**, *7*, 62.
[26] P. Rees, M. R. Brown, H. D. Summers, M. D. Holton, R. J. Errington, S. C. Chappell, P. J. Smith, *BMC Syst. Biol.* **2011**, *5*, 31.
[27] B. D. Chithrani, A. A. Ghazani, W. C. W. Chan, *Nano Lett.* **2006**, *6*, 662.
[28] F. Chen, D. Gerion, *Nano Lett.* **2004**, *4*, 1827.
[29] A. M. Derfus, W. C. W. Chan, S. N. Bhatia, *Adv. Mater.* **2004**, *16*, 961.
[30] F. Fagotto, U. Glück, B. M. Gumbiner, *Curr. Biol.* **1998**, *8*, 181.
[31] K. Ribbeck, D. Görlich, *EMBO J.* **2001**, *20*, 1320.
[32] N. M. Moore, C. L. Sheppard, S. E. Sakiyama-Elbert, *Acta Biomater.* **2009**, *5*, 854.
[33] A. El-Sayed, I. A. Khalil, K. Kogure, S. Futaki, H. Harashima, *J. Biol. Chem.* **2008**, *283*, 23450.
[34] K. Chang, Y. Higuchi, S. Kawakami, F. Yamashita, M. Hashida, *Bioconjug. Chem.* **2010**, *21*, 1087.
[35] J. M. Kogot, H. J. England, G. F. Strouse, T. M. Logan, *J. Am. Chem. Soc.* **2008**, *130*, 16156.
[36] D. Mohr, S. Frey, T. Fischer, T. Güttler, D. Görlich, *EMBO J.* **2009**, *28*, 2541.
[37] P. L. Paine, L. C. Moore, S. B. Horowitz, *Nature* **1975**, *254*, 109.
[38] Y. Williams, A. Sukhanova, M. Nowostawska, A. M. Davies, S. Mitchell, V. Oleinikov, Y. Gun'ko, I. Nabiev, D. Kelleher, Y. Volkov, *Small* **2009**, *5*, 2581.
[39] F. Cardarelli, M. Serresi, R. Bizzarri, M. Giacca, F. Beltram, *Mol. Ther.* **2007**, *15*, 1313.
[40] D. Wang, R. J. Nap, I. Lagzi, B. Kowalczyk, S. Han, B. A. Grzybowski, I. Szleifer, *J. Am. Chem. Soc.* **2011**, *133*, 2192.
[41] Q. Dai, C. Walkey, W. C. W. Chan, *Angew. Chem. Int. Ed.* **2014**, *53*, 5093.
[42] W. C. W. Chan, S. Nie, *Science* **1998**, *281*, 2016.
[43] F. Song, P. S. Tang, H. Durst, D. T. Cramb, W. C. W. Chan, *Angew. Chem. Int. Ed.* **2012**, *51*, 8773.
[44] A. Albanese, K. M. Tsoi, W. C. W. Chan, *J. Lab. Autom.* **2013**, *18*, 99.

Received: April 16, 2014
Revised: May 29, 2014
Published online: July 2, 2014